Progress in Natural Science: Materials International 26 (2016) 404–410

HOSTED BY

Contents lists available at ScienceDirect

Progress in Natural Science: Materials International

journal homepage: www.elsevier.com/locate/pnsmi

Original Research

Preparation of high-performance ultrafine-grained AISI 304L stainless steel under high temperature and pressure

Peng Wang [a], Jinzan Zhang [b], Yang Zhang [a], Haitao Wang [c], Wentao Hu [a], Dongli Yu [a,*]

[a] State Key Laboratory of Metastable Materials Science and Technology, Yanshan University, Qinhuangdao 066004, Hebei, China
[b] Hebei Vocational and Technical College of Building Materials, Qinhuangdao 066004, Hebei, China
[c] China Energy Research Society, Beijing 100045, China

ARTICLE INFO

Article history:
Received 28 January 2016
Received in revised form
6 July 2016
Accepted 6 July 2016
Available online 9 August 2016

Keywords:
AISI 304L stainless steel
Ultra-fine grained bulk
Ball milling
High temperature high pressure
Mechanical properties

ABSTRACT

Bulk ultra-fine grained (UFG) AISI 304L stainless steel with excellent mechanical properties was prepared by a high-temperature and high-pressure (HTHP) method using nanocrystalline AISI 304L stainless steel powders obtained from ball milling. Samples were sintered in high-pressure conditions using the highest martensite content of AISI 304L stainless steel powders milled for 25 h. Analyses of phase composition and grain size were accomplished by X-ray diffraction and Rietveld refinement. By comparing the reverse martensite transformation under vacuum and HTHP treat, we consider that pressure can effectively promote the change in the process of transformation. Compared with the solid-solution-treated 304L, the hardness and yield strength of the samples sintered under HTHP are considerably higher. This method of preparation of UFG bulk stainless steel may be widely popularised and used to obtain UFG metallic materials with good comprehensive performance.

1. Introduction

AISI 304L stainless steel exhibits excellent corrosion resistance and formability and is hence widely employed in industrial applications as an important structural material as well as an engine-related part in the aerospace industry [1–5]. On the downside, the relatively lower strength and specific strength of SS304L stainless steel [6] limit its applications in the field of aviation and aerospace. Hence, improving its strength or specific strength is necessary and will be beneficial to reduce the weight of mechanical parts in aerospace vehicle.

Many routes were employed to improve the strength of metallic materials, such as deformation [7], precipitation [8], solid solution [9], dispersion [10], and grain size reduction [11]. However, only the method of refining grain can simultaneously improve materials' comprehensive performance, including the strength, plasticity and toughness [12–14]. Ball milling is a suitable means to refine grains [15]. Furthermore, high-temperature, high-pressure (HTHP) sintering is effective in controlling grain growth [16].

In this paper, nanocrystalline AISI 304L stainless steel powders were prepared by ball milling method and characterised by X-ray diffraction (XRD). AISI 304L stainless steel blocks were prepared using HTHP sintering method. Their mechanical properties (hardness, strength and plasticity) were studied using mechanical tests. By combining XRD and Rietveld refinement [17], we studied the martensitic and reverse martensitic transformations of AISI 304L stainless steel during ball-milling and HTHP sintering. The influence of the high-pressure condition on the transformation of the inverse martensitic transformation was assessed by comparing the inverse martensitic transformation under vacuum conditions.

2. Experimental

The starting materials used in our study were AISI 304L stainless steel powders purchased from Alfa Asian with a granularity of −400 mesh and chemical composition is listed in Table 1.

The starting materials were ball milled at 400 rpm for different time durations. Ethanol was used as PCA in the ball-milling process, and the ball-to-powder weight ratio was 10:1.

The powder milled for 25 h was loaded into a quartz tube connected to a mechanical pump and molecular pump for vacuum. When the vacuum degree reached 10^{-5} Pa, the electric resistance furnace was used to heat the quartz tube. Thermo-coupling was conducted to control heating, maintaining a predetermined temperature for 15 min. The samples were then cooled with the furnace.

The milled powders were compressed into cylinders (10.7 mm

* Corresponding author.
E-mail addresses: wp@ysu.edu.cn (P. Wang), ydl@ysu.edu.cn (D. Yu).
Peer review under responsibility of Chinese Materials Research Society.

http://dx.doi.org/10.1016/j.pnsc.2016.07.001

Table 1
Chemical composition of the raw materials (mass%).

C	Cr	Ni	Si	Cu	Mo	Mn	Fe
0.03	21.7	10.5	0.68	0.43	0.36	0.2	Balance

in diameter and 9 mm in height), and each cylinder was placed into a hexagonal boron nitride capsule with a 12 mm outer diameter. HTHP experiments were performed using a China-type large volume cubic press that utilises a maximum of 800t for every WC anvil [18]. The samples were firstly compressed to 2.55 GPa pressure and then heated to the desired temperature (200 °C to 800 °C, at intervals of 100 °C) for 15 min by resistive heating with graphite tube heaters (outer diameter of 14 mm and inner diameter of 12 mm). In all the experiments, the temperature was measured in situ with a type K thermocouple (NiCt–NiSi). Pressure was calibrated by the electrical resistance change during the phase transitions of Bi at room temperature [19]. After HTHP treatment, the samples were quenched to room temperature before the pressure was unloaded. Finally, the obtained bulk samples with diameters of approximately 10 mm and heights of 7.5–8 mm were obtained.

Phase identification analysis was conducted using XRD (Rigaku, D/max-2500/PC) with Cu Kα radiation. Prior to XRD examination, the surfaces of the bulk samples were ground with SiC emery papers up to a roughness of 2000 and electro-polished with electrolyte containing 90% acetic acid and 10% perchloric acid at 17 V for 300 s. All of the XRD profiles were normalised against the maximum value. The MAUD software employed for Rietveld refinement was used to calculate the grain sizes and phase fractions. Confidence factor of those fitting were: Rw < 15.0, sig < 2.0. So this accuracy coincided with grain size test standard.

Field emission SEM (HITACHI S-4800) was conducted to observe the microstructures of the powders. The ImageJ software was adopted to calculate the equivalent circle diameter (ECD) of the particles and dimple size.

As cast AISI 304L bar was packaged in an evacuated quartz glass capsule then solution heat treated at 1100 °C for 15 min in furnace and water quenched to prepare solid-solution-treated 304L. It is treated as a contrast sample for mechanical property test.

Vickers hardness test was carried out using a microhardness tester (FUTURE-TECH, FM-ARS9000) with a load of 200 gf for 10 s. The hardness of each sample was tested at 12 points, and the average values and standard deviation were calculated.

The bulk samples and solid-solution-treated AISI 304L bar were cut to cylindrical test specimens with a diameter of 3 mm and height of 4.5 mm through electrical discharge wire-cutting. The compression tests were performed on the sintered samples at the nominal strain rates of 5×10^{-4} at room temperature in air. The tests were performed using a servohydraulic tensile testing machine (Hegewald & Peschke, Inspekt table 100).

3. Results and discussion

3.1. Ball milling of AISI 304L

Fig. 1a shows X-ray profiles for the as-received AISI 304L and samples of AISI 304L milled for 1, 5, 10, 15, 20 and 25 h. Microstructure of the ball-milled specimens consists of a mixture of austenite [γ-phase, face-centred cubic (FCC)] and martensite [α′-phase, body-centred tetragonal (BCT)].

By performing Rietveld refinements using MAUD software [20] on the XRD data, phase fractions and grain sizes were determined at different milling times. The variations are shown in Fig. 1b and c.

Along with increased milling time, the fraction of martensite greatly increased, whereas the fraction of austenite decreased. Therefore, phase transformation from austenite to martensite occurred during ball milling. During mechanical milling, a process that employs severe plastic deformation, high shear strains can lead to strong grain refinement of the treated materials. Under this high strain, the metastable austenite in AISI 304L is prone to change to martensite in a process called strain-induced martensite transformation.

At the start of milling, sufficient powder exhibiting the austenite phase was impacted by the ball, and the martensite phase was then generated rapidly. By increasing the milling time continually, the application of high-velocity impact between the mill ball and powders was repeated. Hence, the amount of transformed martensite increased. With the decrease in amount of the austenite fraction, the probability of collision between the mill ball and powders exhibiting the austenite phase lessened. This result decelerated the increase in amount of the martensite phase. This phenomenon agrees with the results of the XRD refinements in this study.

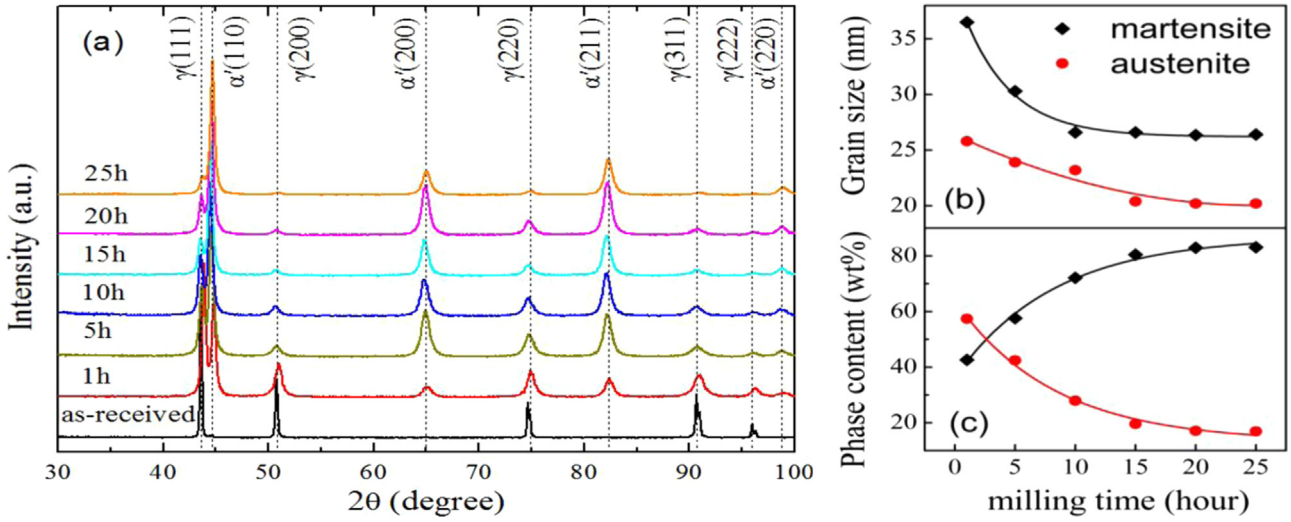

Fig. 1. X-ray diffraction (XRD) spectra and Rietveld refinement results of the as-received AISI 304L and milled powder. (a) XRD spectra of the as-received AISI 304L and samples of AISI 304L milled for 1, 5, 10, 15, 20 and 25 h; (b) relationship between milling time and grain size in the samples; (c) content of martensite and austenite in the milled powder, as calculated by MAUD.

Usually the martensite transformation induced by strain does not transfer completely during plastic deformation. In this study, with the milling time increased to 25 h, the martensite fraction attained equilibrium at about 83%. The adoption of the exponential function is effectively accomplished by curve fitting. With an accuracy of an adjusted R-square of 0.98959 for martensite and 0.99912 for austenite, the effect of milling time on the phase ratio of the milled powders could be represented as follows:

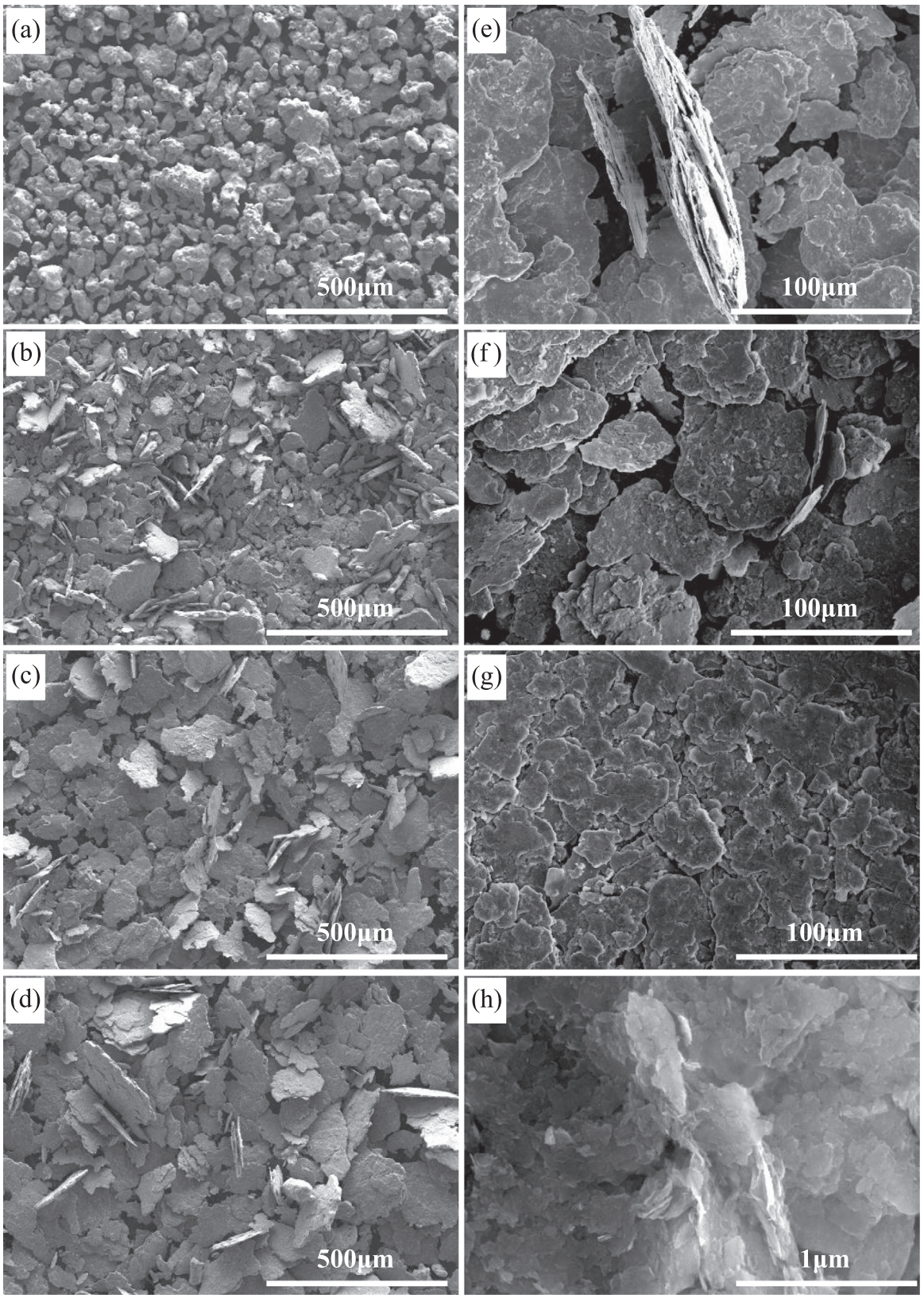

Fig. 2. Surface topography of the raw and milled powders. (a) SEM image of the as-received AISI 304L powder; (b)–(g) SEM images of the AISI 304L powder milled for 1, 5, 10, 15, 20 and 25 h; (h) magnified image of (e).

$$W_M = -50.78719 \times \exp(-t/8.22922) + 86.91899 \quad (1\text{-}1)$$

$$W_A + W_M = 1 \quad (1\text{-}2)$$

where W_M is the weight percent of martensite; W_A is the weight percent of austenite; and t is the milling time, within the range of 1–25.

The martensite ratio of the milled powder was then controlled by manipulating the milling time.

Mechanical milling is considered as an effective grain refinement method. In this work, AISI 304L powders with original grain sizes exceeding 100 nm and martensite were refined to 26 nm after 25 h of milling because martensite exhibits brittleness higher than austenite. During mechanical milling, the austenite phase was firstly transferred to the martensite phase by strain-induced martensite transformation. The more brittle martensite crystal then broke into small fragments, finally resulting in grain refinement.

The grain was refined rapidly at the outset, and the process attained equilibrium after 10 h of milling. This finding agrees with the trend of variation of the weight percent of martensite. Grain refinement and growth are two coupled yet opposing processes. Under certain ball-milling conditions, the change in grain size must terminate at a particular size, and the material must adapt itself to a dynamic equilibrium, such as that of a steady state. The XRD refinement results showed that the grain size of martensite achieved dynamic equilibrium at about 26 nm after 10 h of milling.

Functions 2-1 and 2-2 describe the relationship between grain sizes and milling time. The accuracy of this curve fitting by exponential function is reflected by adjusted R-square of 0.98799 for martensite and 0.90767 for austenite.

$$S_M = 13.38326 \times \exp(-t/3.91769) + 26.20161 \quad (2\text{-}1)$$

$$S_A = 7.84962 \times \exp(-t/13.76406) + 18.56399 \quad (2\text{-}2)$$

where S_M is the grain size of martensite; S_A is the grain size of austenite; and t is the milling time within the range of 1–25.

The surface topography of the milled powders is shown in Fig. 2. The as-received AISI 304L powder shows a ball-like appearance, whereas the milled powders all display plate-like morphologies. The high-power microscopic view demonstrates that these sheets also exhibit a lamellar structure composed of similar smaller pieces, reaching sizes up to the nanometre. This result is due to the repetitive high-velocity impact amongst the milling ball, powders and jar during mechanical milling.

Table 2 shows the changes in mean ECD and thickness of the sheets in the milled powders at different ball-milling durations. At the start of milling, the ball-like particles underwent plastic deformation and eventually became plate-like. As the impact was repeated, the sheets became wider and thicker. When the deformation produced was sufficient, the sheets were split into smaller ones. Finally, the ECD and thickness of the sheets reached a constant. The maximum value of mean ECD during milling was about 132 μm for the 10 h milled powders.

Table 2
Mean ECD and thickness of the sheets in the powders during milling.

Milling time (h)	Mean ECD (μm)	Thickness (μm)
0	20	~20
1	78	~15
5	103	~5
10	132	~5
15	70	~3
20	56	~3
25	45	~3

During ball milling, we utilised ethanol as a process control agent (PCA) to improve the output rate of milled powders and promote grain refinement. From the XRD and scanning electron microscopy (SEM) analyses, we found that the powders obtained in this work were composed of nanoscaled grains and micron-scaled sheets comprising nanoscaled pieces.

3.2. Vacuum and HTHP treatment of milled powder

Fig. 3a reveals the XRD patterns of the powder milled for 25 h and samples treated in a vacuum annealing furnace for 15 min from 300 °C to 800 °C. The Rietveld refinement results are shown in Fig. 3b and c.

Fig. 4a displays the XRD profile of a series of HTHP samples. The precursor adopted was the 25 h milled AISI 304 L powder. This sample was treated 15 min under a pressure of 2.55 GPa, and the temperatures range from 200 °C to 800 °C. Fig. 4b and c display the Rietveld refinement results of the XRD data.

By comparing Figs. 3 and 4, it can be noted that with the increase in sintering temperature, both revealed decreased contents of the martensite phase and increased contents of the austenite phase. This finding shows that the inverse martensitic transformation of the martensite phase to the austenite phase occurs during the sintering process.

Meanwhile, the difference between the two conditions lies in the temperature range of the inverse martensitic transformation. During the process of vacuum heat treatment, the inverse martensitic transformation was initiated at 500 °C and at the end of 800 °C. By contrast, in high-pressure heat treatment, the inverse martensitic transformation began at 400 °C and ended at 600 °C.

Patel and Cohen [21] have been discussed quantitatively about the effect of an external force on martensitic transformations. They reported, the mechanical work, ΔG_{a-m}, done on the system by hydrostatic pressure is written as:

$$\Delta G_{a-m} = (V_a - V_m)P \quad (3\text{-}1)$$

And in the inverse martensitic transformations:

$$\Delta G_{m-a} = (V_m - V_a)P \quad (3\text{-}2)$$

where V_a and V_m are the volume of austenite and martensite, respectively. P is the pressure of the system, takes a negative value, under the condition of compressive stress. The austenite phase is an FCC structure, with the largest atomic packing density. However, the crystal structure of the martensite phase was in structure BCT, and the atomic packing density was smaller, and therefore $V_m - V_a$ become a positive value. Thus, $\Delta G_{m-a} < 0$, pressure decreases the free energy necessary for the inverse martensitic transformation to occur. Therefore, the high pressure reduces the initial temperature of the reverse martensitic transformation and shortens the phase transition temperature range.

Ball milling powder has the characteristics of nanoscaled grain size, high micro-strain, high dislocation density and high deformation storage energy. From the Gibbs Thomson equation [22] describing the grain growth theory shows that grain growth driving force is inversely proportional to grain size. When the grain size of the milled powders reached a nanometre scale, the larger driving force will promote the boundary rearrangement and grain growth under the lower treating temperature. In this experiment, the 304L stainless steel nanocrystals have grown up at 300 °C, which is consistent with the results of pure Fe and Ni nanocrystals growth reported in the literature [23,24].

From Figs. 3c and 4c, it can be found that in the two conditions,

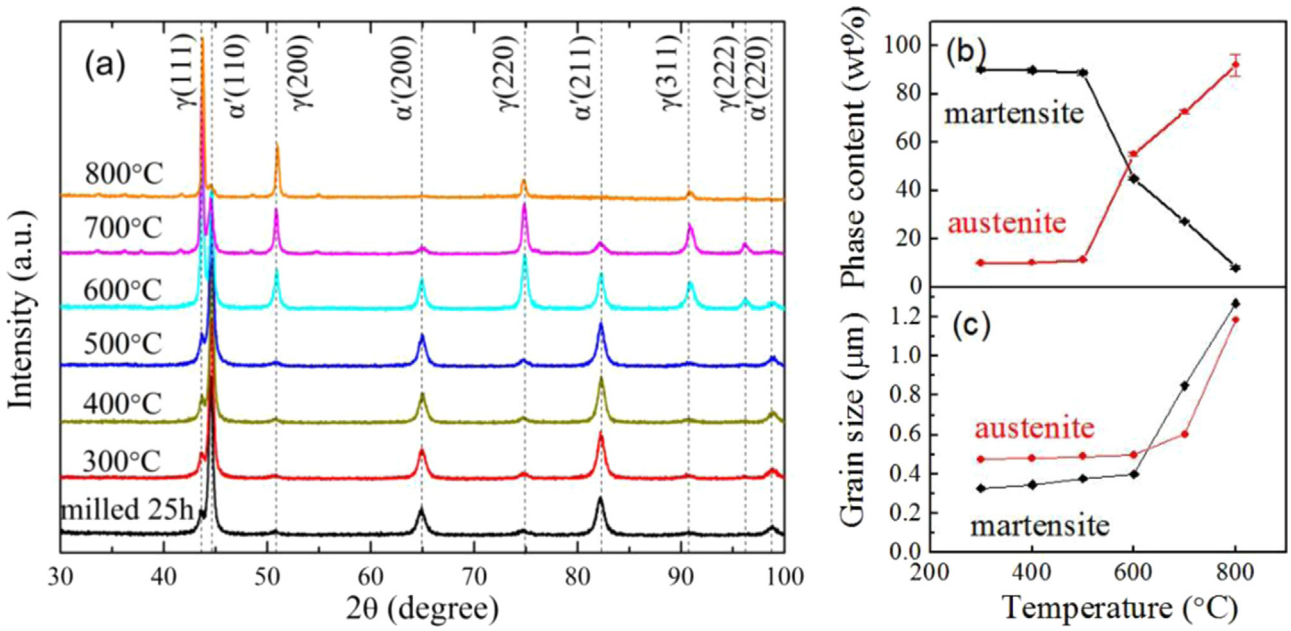

Fig. 3. XRD spectra and Rietveld refinement results of powder milled for 25 h and its vacuum heat-treated samples. (a) XRD spectra of the samples subjected to vacuum heat treatment at 300 °C to 800 °C (at intervals of 100 °C); (b) trend of variation of the martensite and austenite contents with temperature; (c) relation of the grain sizes of the martensite and austenites with the change in temperature, as calculated by MAUD.

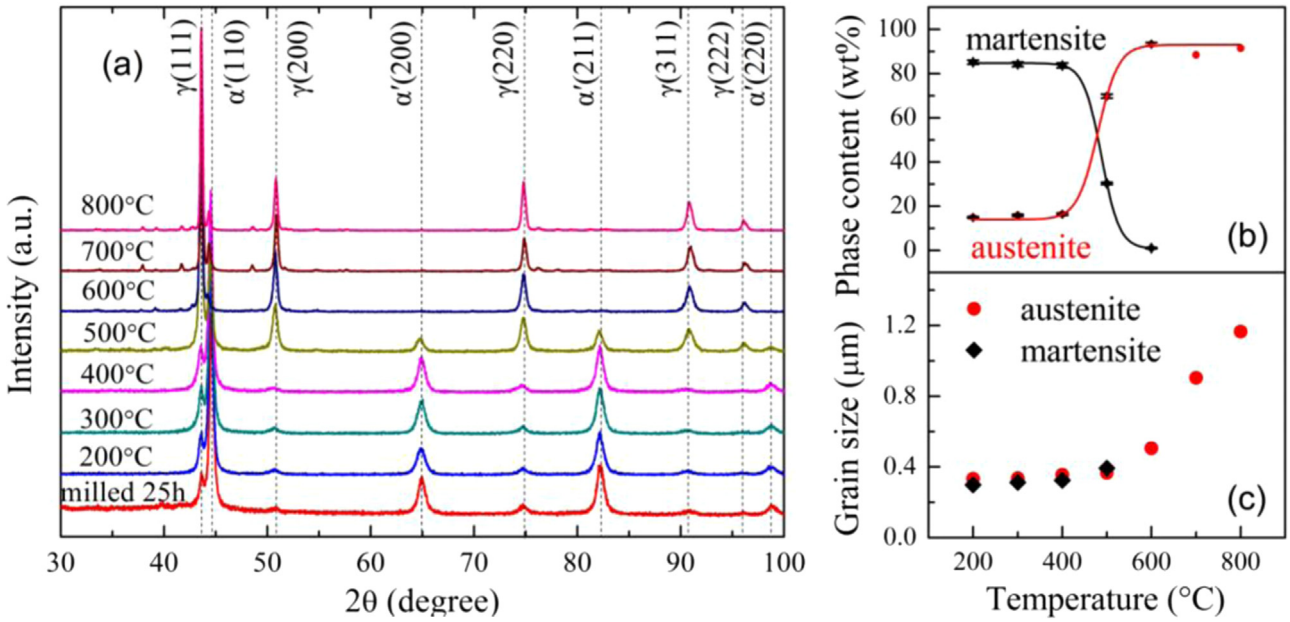

Fig. 4. XRD spectra and Rietveld refinement results of the powder milled for 25 h and its HTHP samples. (a) XRD spectra of the samples heat treated under 2.55 GPa and temperature range of 200 °C to 800 (at intervals of 100 °C); (b) trend of variation of the martensite and austenite contents with temperature; (c) relation of the grain sizes of the martensite and austenites with the change in temperature, as calculated by MAUD.

the law of grain size change with temperature is consistent. The grain sizes for all samples rapidly grew up at 600 °C. Based on above phase change dynamics analysis, we know that the pressure can promote inverse martensite phase transformation. Hence, these results show that pressure reduce the initial transition temperature and shorten the transition temperature range, which lead to forming ultrafine grained austenitic stainless steel by quickly completing phase transformation before the grains growing up.

The Boltzmann function is used to fit the mass fraction of the austenite phase in Fig. 4b. The accuracy of this curve fitting was reflected by an adjusted R-square of 0.99972. The trend of variation of the austenite phase content with the change in sintering temperature can be expressed by the following formula:

$$W_A = 92.98065 - 79.05831/(1 + \exp\left[(T_A - 479.88232)/22.92602\right] \quad (4\text{-}1)$$

where W_A is the weight percent of austenite and T_A is the sintered temperature within the range of 200–800.

Eq. (4-2) shows the relationship between the phase content of the martensite and the change in sintering temperature.

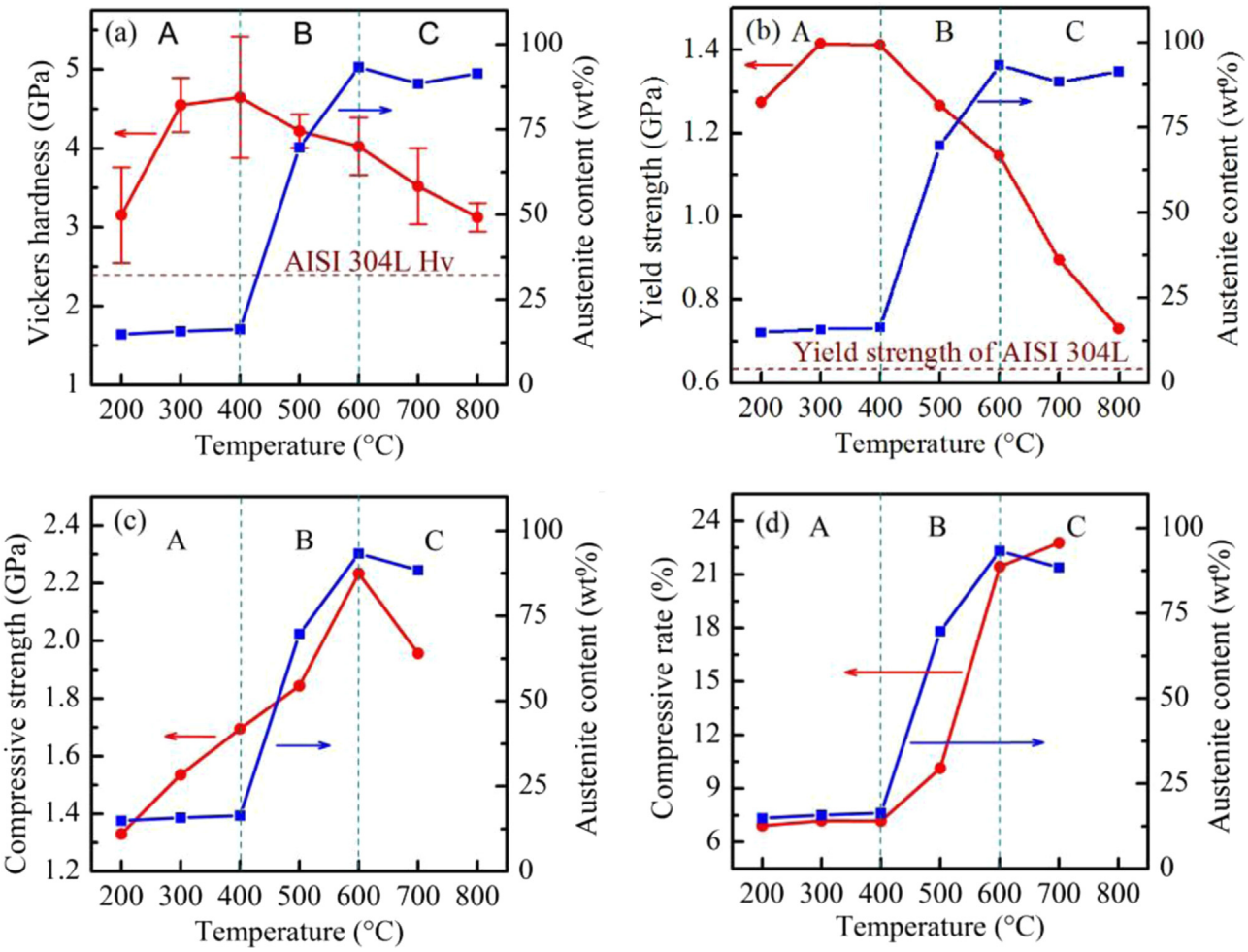

Fig. 5. Mechanical properties of HTHP samples. (a) Vickers hardness and (b) yield strength of HTHP samples; solid-solution-treated AISI 304L and its corresponding phase contents; (c) compressive strength and (d) compressive rate of the HTHP samples and the corresponding phase contents.

$$W_M = 0.49559 + 84.77136/(1 + \exp\left[(T_M - 486.50285)/21.99038\right] \quad (4\text{-}2)$$

where W_M is the weight percent of martensite and T_M is the sintered temperature within the range of 200–600.

3.3. Mechanical properties of the HTHP samples

In this work, the HTHP sample was exceedingly small for the tensile test. Hence, the compression test was adopted to test the samples' mechanical properties. Afterward, the samples were polished for the micro Vickers hardness test. The solid-solution-treated AISI 304L was tested in the same conditions for comparison. The results and the corresponding phase contents are shown in Fig. 5. Red line in the figure represents the corresponding mechanical properties of the sample, and the blue line is the changing rule of the austenite phase content in the sample.

We found that the HTHP samples possess higher hardness values than those of the solid-solution-treated AISI 304L. Amongst the samples, those sintered at 400 °C achieved the greatest hardness, 4.65 GPa, which was nearly twice as much as the hardness of the solid-solution-treated AISI 304L. The yield strengths in all samples obtained under HTHP conditions were higher than those of the solid-solution-treated AISI 304L. Amongst the samples, those sintered at 400 °C attained the highest yield strength, 1412 MPa, and were almost four times that of the solid-solution-treated 304L yield strength. However, the compression ratio of sintered samples at 400 °C is only 7.5%, and the ductility is poor. Considering the toughness of the material, the sample sintered at 600 °C has the best comprehensive performance. Its hardness and yield strength was increased by 72% and 224%, compared with the solid-solution-treated AISI 304L, respectively. At the same time, its compressive strength reaches 2233 MPa; the compression rate is 21.4%.

Considering the changes in phase content and mechanical properties, we divide the results into three regions for analysis and discussion. The region covered by 200 °C to 400 °C was denoted as the A region. In this group, the main phase of the sample is martensite phase, and the phase content is almost constant. Therefore, the procedures applied are a sintering and densified process. A large number of martensite improved the hardness and yield strength of the samples. With the increasing sintering temperature, all of the mechanical performance indices increased.

Meanwhile, the region from 400 °C to 600 °C corresponds with the B region, which displays a sharp reverse martensitic transformation in the sample. The newly generated austenite has a lower strength and better malleability than the intrinsic martensite. Thus, the hardness and yield strength decrease with the decrease in the martensite content. At the same time, the compressive strength and rates increase.

In samples sintered at 600 °C and above, the martensite contained in the sample was completely decomposed. The region

from 600 °C to 800 °C was regarded as the C region, in which the sample is in the austenite phase. Fig. 4b shows that the austenite grain size increased from 400 nm to 1500 nm at the C stage. Grain growth decreases inner stress and generates a softening effect. Hence, the hardness, yield strength and compressive strength decrease.

The compression rate is more sensitive to the fraction of austenite than the grain size. Therefore, the fraction of austenite increases and the compression rate continues to increase with the increase in sintering temperature. In this compression test, we found that the ductility is sufficient such that the samples cannot be fractured in the compression process. Thus, the samples do not achieve the compression strength and compression ratio of the samples. This finding must be validated to improve the sample size in the following experiments, and the tensile test must be used in future investigations.

4. Conclusions

(1) The nanocrystalline AISI 304L stainless steel powders were successfully prepared by the ball-milling method. Using powder with the highest martensite content as raw materials, the UFG austenitic stainless steel bulk was obtained under HTHP conditions.
(2) Pressure can reduce the initial temperature and shortens the temperature range of reverse martensitic transformation in AISI 304L, cause the pressure can decrease the free energy necessary for the transformation to occur.
(3) Under the condition of 2.55 GPa pressure and high temperature of 600 °C, the bulk UFG of austenitic stainless steel with excellent mechanical properties, including high hardness and yield strength, can be prepared,.

Acknowledgements

This work was supported by the National Natural Science Foundation of China (51031002).

References

[1] A.J. Sedric, Corrosion of Stainless Steels, 2nd ed., John Wiley & Sons, New York, 1996.
[2] C. Tide, S.R. Harkin, G.G. Geesey, P.J. Bremer, W. Scholz, J. Food Eng. 42 (1999) 85–96.
[3] W. Liu, R.J. Wang, J.L. Han, X.Y. Xu, Q. Li, J. Mater. Process. Technol. 210 (2010) 1956–1961.
[4] M. Finsgar, I. Milosev, Corros. Sci. 52 (2010) 2430–2438.
[5] W. Kuang, E.H. Han, X. Wu, J. Rao, Corros. Sci. 52 (2010) 3654–3660.
[6] The Materials Information Society, ASM Specialty Handbook: Stainless Steel, ASM International, Metals Park, OH, 1994.
[7] E.P. Degarmo, J.T. Black, R.A. Kohser, Materials and Processes in Manufacturing, 9th ed., Wiley, Hoboken, N.J., 2003.
[8] W.D. Callister, Fundamentals of Materials Science and Engineering, 2nd ed., Wiley & Sons, Hoboken, N.J., 2004.
[9] B. Sun, S.F. LI, H. Imai, T. Mimoto, J. Umeda, K. Kondoh, Mater. Sci. Eng.: A 563 (2013) 95–100.
[10] S. Ukai, T. Kaito, S. Ohtsuka, T. Narita, M. Fujiwara, ISIJ Int. 43 (2003) 2038–2045.
[11] Y.M. Wang, E. Ma, Mater. Sci. Eng. A 375 (2004) 46–52.
[12] Y.M. Wang, M.W. Chen, F.H. Zhou, et al., Nature 419 (2002) 912–915.
[13] V. Ruslan, Nature 419 (2002) 887–889.
[14] L. Lu, Y. Shen, X. Chen, L. Qian, K. Lu, Science 304 (2004) 422–426.
[15] M. Stubicar, Z. Blazina, A. Tonejc, N. Stubicar, D. Krumes, Physica B 304 (2001) 304–308.
[16] Y.J. Tian, B. Xu, D.L. Yu, et al., Nature 493 (2013) 385–388.
[17] H.M. Rietveld, J. Appl. Cryst. 2 (1969) 65–71.
[18] X. Liu, J.L. Chen, J.J. Tang, et al., High. Press. Res. 32 (2012) 239–254.
[19] D.L. Decker, W.A. Bassett, L. Merrill, H.T. Hall, J.D. Barnett, J. Phys. Chem. Ref. Data 1 (1972) 773–835.
[20] L. Lutterotti, Nucl. Instrum. Methods Phys. Res. B 268 (2010) 334–340.
[21] J. Patel, M. Cohen, Acta Metall. 1 (1953) 531–538.
[22] P.G. Shewmon, Transformation in Metals, Mc Graw-Hill Book Co., New York 1969, p. 116.
[23] R.A. Andrievski, J. Mater. Sci. 38 (7) (2003) 1367–1375.
[24] B.S. Murty, M.K. Datta, S.K. Pabi, Sadhana 1–2 (28) (2003) 23–45.